Neutral pion to two-photons transition form factor revisited

M. Atif Sultan,[1,2,*] Jiayin Kang,[1,†] Adnan Bashir,[3,4,‡] and Lei Chang[1,§]

[1]*School of Physics, Nankai University, Tianjin 300071, China*
[2]*Centre For High Energy Physics, University of the Punjab, Lahore (54590), Pakistan*
[3]*Instituto de Física y Matemáticas, Universidad Michoacana de San Nicolás de Hidalgo, Morelia, Michoacán 58040, México*
[4]*Department of Integrated Sciences and Center for Advanced Studies in Physics, Mathematics and Computation, University of Huelva, E-21071 Huelva, Spain*

(Received 17 September 2024; accepted 5 December 2024; published 30 December 2024)

Based upon a combined formalism of Schwinger-Dyson and Bethe-Salpeter equations in quantum chromodynamics (QCD), we propose a QCD-kindred algebraic model for the dressed quark propagator, for the Bethe-Salpeter amplitude of the pion and the electromagnetic quark-photon interaction vertex. We then compute the $\gamma^*\pi^0\gamma$ transition form factor $G^{\gamma^*\pi^0\gamma}(Q^2)$ for a wide range of photon momentum transfer squared Q^2. The quark propagator is expanded out in its perturbative functional form but with dynamically generated dressed quark mass. It has complex conjugate pole singularities in the complex-momentum plane, which is motivated by the solution of the quark gap equation with rainbow-ladder truncation of the infinite set of Schwinger-Dyson equations. This complex pole singularity structure of the quark propagator can be associated with a signal of confinement, which prevents quarks from becoming stable asymptotic states. The Bethe-Salpeter amplitude is expressed without a spectral density function, which encapsulates its low- and large-momentum behavior. The QCD evolution of the distribution amplitude is also incorporated into our model through the direct implementation of Efremov-Radyushkin-Brodsky-Lepage evolution equations. We include the effects of the quark anomalous magnetic moment in the description of the quark-photon vertex, whose infrared enhancement is known to dictate hadronic properties. Once the QCD-kindred model is constructed, we calculate the form factor $G^{\gamma^*\pi^0\gamma}(Q^2)$ and find it consistent with direct QCD-based studies, as well as most available experimental data. It slightly exceeds the conformal limit for large Q^2, which might be attributed to the scaling violations in QCD. The associated interaction radius and neutral pion decay width turn out to be compatible with experimental data.

DOI: 10.1103/PhysRevD.110.114047

I. INTRODUCTION

Quantum chromodynamics (QCD) [1], the theory of strong interactions, is perhaps the most intriguing and challenging piece of the standard model of elementary particles. Recall that all the QCD elementary degrees of freedom, quarks and gluons, lie in the fundamental and the adjoint representation, respectively, of the $SU(3)$ color gauge group. Therefore, it is a non-Abelian gauge theory—it is renormalizable and it exhibits asymptotic freedom [2,3] in its perturbative tail. This feature allows us to study strong interaction processes using the well-established Feynman diagrammatic approach at an energy scale sufficiently greater than its intrinsic hadronic scale $\Lambda_{\rm QCD}$. However, in the infrared region, strong coupling is of order one or higher, which makes the perturbative approach inapplicable. Therefore, at this energy scale, one is forced to resort to intrinsically nonperturbative methods, such as lattice simulation of QCD [4] and a coupled formalism of Schwinger-Dyson (SDEs) and Bethe-Salpeter equations (BSEs) [5,6].

All hadronic observables may be calculated if we know the Green functions of QCD, which satisfy a set of infinite, coupled, nonlinear integral equations, the already mentioned SDEs [6,7]. The mathematical structure of these equations is such that the two-point one-particle irreducible (1PI) Green functions (quark, gluon, and ghost propagators) are related to the three-point functions (for example, quark-gluon and triple-gluon vertices), which in turn are intrinsically entangled with the four-point functions ($2 \to 2$ scattering kernels), *ad infinitum*. This fundamental and

*Contact author: atifsultan.chep@pu.edu.pk
†Contact author: kangjiayin@mail.nankai.edu.cn
‡Contact author: adnan.bashir@umich.mx
§Contact author: leichang@nankai.edu.cn

accurate description of QCD through its SDEs is not limited to its perturbative domain. However, in the weak coupling regime of QCD, this formalism reduces to the well-known order-by-order perturbative expansion of the S matrix of the theory. Even more interestingly, in the nonperturbative domain of QCD, emergent phenomena of confinement and dynamical mass generation, inaccessible in perturbation theory, emanate naturally through realistic studies of the SDEs. Reliable extraction of physical observables in any nonperturbative formalism of QCD is cumbersome and prone to methods that are less systematic and robust than perturbation theory. In this article, we employ the coupled SDE/BSE formalism. Before attempting any solution within this approach, the infinite set of equations must be truncated by introducing mathematical model(s) of some suitable set of Green functions. That is why modeling remains a crucial component in hadron physics. However, despite this challenge, remarkable progress has been made, and QCD-akin truncations offer increasingly precise solutions [8–13]. Fortunately, our understanding of the intricate interplay between the quark propagator and the meson's BS amplitude (BSA) [14] enables us to build their models, which are amicable enough to allow for algebraic manipulations while still producing reliable predictions for the physical observables. In this article, we construct a QCD-kindred algebraic model (QAM) for the pion. Most algebraic models to date shuffle the momentum dependence of the quark propagator and that of the BSA so as to simplify algebraic manipulation to compute hadronic observables. We present the construction of the QAM, which embodies the following key properties:

(i) The quark propagator incorporates its confining features. It is expanded in terms of complex conjugate poles, which are present on the timelike half of the complex momentum plane. The existence and location of these poles resonates with more elaborate studies of the QCD SDEs.
(ii) The momentum dependence of the quark propagator in our model is akin to the QCD-kindred truncations of SDEs. The mass function saturates in the infrared domain, while it falls off as $1/p^2$ in the ultraviolet domain, which agrees with its perturbative behavior up to QCD logarithms in the chiral limit.
(iii) We put forward a simple QAM for the leading pion BSA, which again encodes its low- and large-momentum behavior.
(iv) The model guarantees that the axial vector Ward identity is observed, thus ensuring that the Goldberger-Treiman relation connecting the quark propagator with the BSA is satisfied.
(v) To study the pion with electromagnetic probes, we also require the quark-photon vertex (QPV), for which we add to the usual γ_μ part a transverse vertex containing anomalous magnetic moment (AMM) distribution, which is known to affect the infrared limits of form factors.
(vi) The QAM in its totality ensures that the Abelian anomaly is correctly reproduced at $Q^2 = 0$.
(vii) We explicitly show that the large Q^2 power law for the transition form factor (TFF) is correctly reproduced in accordance with the expectations of asymptotic QCD up to the logarithms, which stem from the running of the strong interaction coupling.
(viii) Finally, our constructed QAM takes into account the Efremov-Radyushkin-Brodsky-Lepage (ERBL) evolution equations for the pion distribution amplitude (DA).

Note that the precise shape of the pion DA to be determined is an intriguing topic that has been studied using numerous approaches, e.g., the QCD sum rules, the lattice QCD, the SDEs, etc. [15–19]. DAs play an essential role in describing various hard exclusive processes of QCD [20–22], such as the electromagnetic form factors (EFFs) and TFFs [20,23], diffractive vector-meson production [24,25], as well as in the study of CP violation via the nonleptonic decays of heavy-light mesons [26,27], etc. We then employ our model to compute the pion TFF to two photons ($\gamma\gamma^*$).

Chiral anomaly fixes the value of the pion TFF at the origin $Q^2 = 0$, while its behavior at large values of momentum transfer Q^2 has been predicted through asymptotic QCD. Therefore, it is a particularly important transition that studies the internal structure of the neutral pion both in the infrared and ultraviolet domains of QCD through one single physical observable. Until 1998, the CELLO [28] and CLEO [29] data were available for the pion TFF in the spacelike region $Q^2 < 7$ GeV^2. *BABAR* collaboration [30] released data on the pion TFF for the spacelike region $Q^2 \in [4,40]$ around the end of 2009. These data initiated a contentious debate by suggesting the TFF's unexpected scaling violation through a power law instead of the usual much milder QCD logarithms. Their measured results show a rapid growth of $Q^2 G^{\gamma^*\pi^0\gamma}(Q^2)$ for the region $Q^2 > 15$, which contradicts the well-known asymptotic prediction that $Q^2 G^{\gamma^*\pi^0\gamma}(Q^2) \to$ constant for large Q^2 up to QCD logarithms. It took several works, which immediately followed, to suggest that the *BABAR* data might not be an accurate measure of the pion TFF [31–34]. In support of these predictions, the subsequent Belle collaboration measurements in 2012 for the same energy region do not reconcile well with the *BABAR* data [35]. Their data clearly seem to indicate that $Q^2 G^{\gamma^*\pi^0\gamma}(Q^2) \to$ constant for large Q^2. This was confirmed later by the QCD-akin SDE computations [36] and the recent data-driven calculation [37]. Hopefully, at the experimental level, the Belle II at SuperKEKB experiment [38], with less uncertainty at large Q^2, will be helpful to clarify the above experimental discrepancy. The aim of this work is to reexamine these varying claims using an updated investigation of the pion TFF with a QAM of the quark propagator, BSA, and DA.

Recall that in Ref. [36], refined calculations were performed using a model parametrization of the QCD-akin

quark propagator and the quark-photon vertex together, incorporating the spectral density in the specific Nakanishi representation of the BSA. In contrast, the present work adopts simpler models for the quark propagator, quark-photon vertex, and the BSA, without relying on a spectral density function. We argue that this exercise is valuable for several reasons. Firstly, these simplified, yet physically motivated, and reliable models make the calculations more tractable while still yielding the correct value for the chiral anomaly, the large photon-virtuality behavior, and results that agree rather satisfactorily with the available experimental data. Secondly, the DA calculated with these models shows good agreement with the predictions from the SDEs. The qualitative and quantitative behavior of the DA is captured by the momentum dependence of the quark mass function and the Bethe-Salpeter amplitude, rather than being controlled by an *ad hoc* choice of spectral density for the BSA. Furthermore, the evolution of the DA can be studied at the level of the propagator and amplitude, allowing exploration of scaling violation phenomena directly. Finally, this approach can be extended to other areas of physical interest with ease, such as the electromagnetic properties of kaons and the axial-vector meson transition form factor to two photons, among others.

It might be worth recalling the importance and impact of the pion TFF to two photons in the precision studies of the celebrated standard model of particle physics. The hadron light-by-light contribution coming from the neutral pion transition to two photons is the most dominant to the anomalous magnetic moment of the muon [39,40]. Therefore, an accurate prediction of this observable is important in the precision studies of the standard model [41].

The article is organized as follows: in Sec. II, we introduce the QAM of the quark propagator and the leading pion BSA. We also present in detail the QPV with the AMM transverse to the photon momentum. In Sec. III, we discuss the pion DA and its QCD evolution. In Sec. IV, we study, compute, and report the $\gamma^*\pi^0\gamma$ TFF—in particular, its connection with chiral anomaly, its asymptotic behavior in QCD, and a comparison with experimental data. We also explain the effect of the AMM term on pion TFF and the Abelian anomaly. Finally, in Sec. V, we present our conclusions and final remarks.

II. FORMALISM

The BSE [42,43] provides the full relativistic description of meson-bound states, which appear as poles for specific values of invariant masses in BSA, and these masses depend on the quantum numbers of the given meson state. The solution of the BSE,

$$[\Gamma_M(p;P)]_{tu} = \int \frac{d^4k}{(2\pi)^4} K^{rs}_{tu}(p,k;P) \times (S_a(k_+)\Gamma_M(k;P)S_b(k_-))_{rs}, \quad (1)$$

provides the BSA, i.e., the one-particle irreducible quark-meson vertex $\Gamma^{ab}_M(p;P)$, where a and b represent the flavors of the quark and the antiquark, respectively, and r, s, t, and u collectively stand for the color and Dirac indices. Here, M only specifies the type of the meson. The momentum conservation implies that $p_\pm = p \pm \eta_\pm P$ and $k_\pm = k \pm \eta_\pm P$, which satisfies the condition $\eta_+ + \eta_- = 1$. The renormalized, amputated quark-antiquark kernel K is irreducible with respect to cutting a pair of quark-antiquark lines. The kernel K is the physical input to BSE along with the quark propagator, and we must specify it in order to solve the BSE for the meson mass and the BSA. For a comprehensive review of the SDE-BSE formalism and its applications to hadron physics, see Refs. [44–47].

The a-flavor-dressed quark propagator S_a is obtained as the solution of the quark SDE [45,48–51]

$$S_a^{-1}(p) = (i\not{p} + m_a) + \frac{4g^2}{3} \times \int \frac{d^4k}{(2\pi)^4} D_{\mu\nu}(p-k)\gamma_\mu S_a(k)\Gamma_\nu(k,p). \quad (2)$$

Here, m_a is the a-flavor current quark mass and g is the strong interaction coupling constant appearing in the Lagrangian. The rest of the components of Eq. (2) are defined as usual: the symbols $D_{\mu\nu}$ and Γ_ν, respectively, are the fully dressed gluon propagator and the QPV, each of which satisfy their own SDE. The eventual goal is to obtain the solution of the BSE by solving it in a coupled form along with the SDEs of the gluon propagator and the QPV. This is a prohibitively tough problem to solve and such a study is beyond the scope of this work. Despite this impediment, many studies have been carried out that unveil the nonperturbative structure of these additional functions through QCD symmetries and/or directly using their corresponding SDEs [52–55]. Lattice formulation of QCD also provides useful insight [56–59]. Despite the fact that sophisticated, robust, and reliable solutions for the propagators and BSA can be obtained from the corresponding SDEs and BSEs, less complicated models can be constructed that capture the essence of infrared aspects of strong interactions, constrained by the requirements of asymptotic QCD [51,60,61]. Our effort includes realistic and explicit momentum dependence of the quark propagator, implements confinement, and provides a simple yet physically sensible description of the pion BSA, as discussed in the subsections below.

A. Constructing the model

A simple but efficacious model of the quark propagtor, the BSA, and the QPV can be constructed to algebraically compute electromagnetically probed physical observables related to the pion.

1. The quark propagator

A simple but physically sensible *Ansatz* for the momentum-dependent quark propagator can be written as follows:

$$S^{-1}(k) = i\gamma \cdot k + B(k^2), \tag{3}$$

with the running quark mass function [62]

$$B(k^2) = \frac{yM^3}{k^2 + yM^2}, \tag{4}$$

which saturates in the infrared domain to a constituent mass $B(0) = M$ and drops off as $1/p^2$ in the ultraviolet domain, as dictated by perturbation theory, save the logarithmic corrections. Here, y is a parameter that controls the width of the mass function. In order to mimic confinement efficaciously, the *Ansatz* in Eq. (4) can be extended into the complex plane by requiring it to be expanded into a sum of a few complex conjugate pole representations,

$$S(k) = \sum_{j=1}^{3} \frac{-i\gamma \cdot k\alpha_j + \beta_j M}{k^2 + \gamma_j M^2} \equiv -i\gamma \cdot k\sigma_A(k^2) + \sigma_B(k^2). \tag{5}$$

Comparing Eqs. (3)–(5) and allowing for the complex poles leads to the identification of γ_j and α_j, β_j. It has long been known that the usually employed rainbow-ladder (RL) truncation to the quark propagator SDE does produce complex conjugate singularities on the timelike half of the complex momentum plane, which can be linked to confinement. Our present model for the quark propagator mimics these singularities, which play an essential role in this work. Such representation also allows us to directly calculate the form factors for large-momentum regions [63].

2. Bethe-Salpeter amplitude

We propose a simple momentum-dependent BSA model for the pion without considering the so-called spectral density function,

$$\Gamma(k; P) = i\gamma_5 \frac{1}{f_\pi} \frac{yM^3}{k^2 + yM^2}, \tag{6}$$

where k is the relative $\bar{q}q$ momentum and f_π is the leptonic decay constant of the pion. At $P = 0$, i.e., in the soft pion limit, we recuperate the exact Goldberger-Treiman relation

$$\Gamma(k; P = 0) = i\gamma_5 \frac{B(k^2)}{f_\pi}, \tag{7}$$

where $B(k^2)$ is the Lorentz scalar mass function appearing in the quark inverse propagator, Eq. (4), thus already connecting the BSA of the pion with the quark propagator.

3. Quark-photon vertex

It has been known for a long time that the longitudinal Ball-Chiu (BC) vertex *Ansatz* [64] could ensure chiral anomaly by construction [65,66]. Although we could naturally incorporate the BC vertex into our model, it has also long been established that without the appropriate transverse pieces of the vertex [67,68], the BC vertex is not entirely reliable. As a result, it is noticed that in the intermediate photon momentum region, the calculated form factor is too hard [69]. Therefore, we prefer our proposed QPV, which includes a transverse AMM part. Our construction consists of the bare vertex augmented by a part transverse to the photon momentum adapted from the *Ansatz* [70,71]

$$\Gamma_\mu(p, q) = \gamma_\mu - \sigma_{\mu\nu}(p - q)_\nu \frac{B(p) - B(q)}{p^2 - q^2} \mathcal{H}(Q^2), \tag{8}$$

where $\mathcal{H}(Q^2) = \eta(1 - \exp[-Q^2/\hat{M}^2])/(Q^2/\hat{M}^2)$. The second term can be regarded as the dynamically generated nonperturbative analogue of the Pauli form factor for the AMM term [68,72]. Note that $\mathcal{H}(Q^2)$ is independent of the relative momentum of the quark and antiquark, and thus depends only on the photon momentum squared Q^2. The parameter $\hat{M}$ can be used to adjust the pion interaction radius.

It is worth noting that the dressing function $\mathcal{H}(Q^2)$ of the AMM term is proportional to the strength parameter η. The AMM term disappears for the $\eta = 0$ limit and $\mathcal{H}(Q^2) \to 0$ as $Q^2 \to \infty$. All these features of the $\mathcal{H}(Q^2)$ dressing function become more perceptible in Fig. 1, which depicts its profile in a pertinent momentum range. Therefore, as we discuss in detail in Sec. IV, the AMM term could indeed contribute to the chiral anomaly in the $\gamma^*\pi^0\gamma$ transition TFF quantitatively.

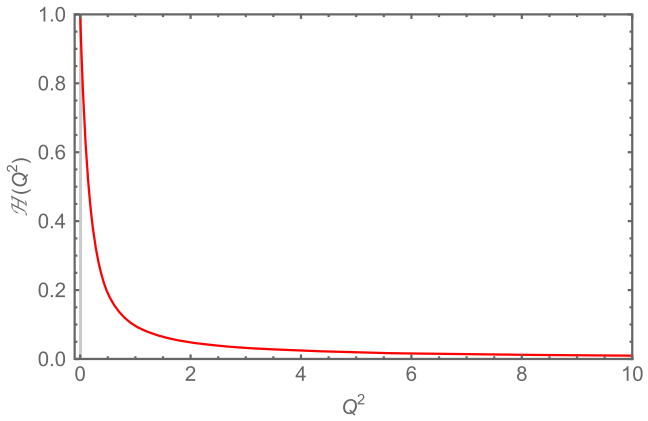

FIG. 1. The QPV dressing function $\mathcal{H}(Q^2)$ for the AMM contribution with $\hat{M} = 0.3105$ GeV and $\eta = 1$.

III. PION DISTRIBUTION AMPLITUDE AND THE MODEL PARAMETERS

The pion TFF is sensitive to the shape of the pion DA. The precise behavior of the pion DA is an intriguing issue that has been addressed using numerous approaches, e.g., the QCD sum rules, the Lattice QCD, the SDEs, etc. [16,18,73–76]. Following the standard definition of the DA [77] and the practical operation process [78], we can obtain the following analytical representation of the DA with the input of the quark propagator and BSA in the chiral limit:

$$\varphi(x) = \frac{3yM^2}{2f_\pi^2\pi^2}\sum_{j1,j2}\frac{x\alpha_{j1}\beta_{j2}+(1-x)\alpha_{j2}\beta_{j1}}{2y-\gamma_{j1}-\gamma_{j2}} \times\left\{\log\left[\frac{2y(1-x)-(1-2x)\gamma_{j2}}{(1-x)\gamma_{j1}+x\gamma_{j2}}\right]\theta\left(x-\frac{1}{2}\right) + \log\left[\frac{2yx+(1-2x)\gamma_{j1}}{(1-x)\gamma_{j1}+x\gamma_{j2}}\right]\theta\left(\frac{1}{2}-x\right)\right\}. \quad (9)$$

We find that the proper choice of the parameter y can produce different DAs at 2 GeV. We choose two sets of parameters that reproduce the same value of f_π and yield the second moment $\langle(2x-1)^2\rangle = 0.25(0.01)$ of the pion DA based on an earlier SDE prediction [79]. In Table I, we present these best two sets of parameters at 2 GeV, the computed f_π, and the second moment of the PDA.

We depict the pion DAs in Fig. 2, and compare with the asymptotic two-particle DA $\phi_{asy}(x) = 6x(1-x)$ and the SDE prediction. Owing to the dominance of dynamical chiral symmetry breaking (DCSB), pion DA is rather dilated, exhibits a significant deviation from $\phi_{asy}(x)$, and has good agreement with the SDE prediction [79]. All the DAs are symmetrical in Fig. 2. Historically, in the constituent quark mass algebraic models, the spectral density is introduced in the BSA to produce broad DA. However, in the present work, we find that the broad DA can be produced without the specific choice or even recourse to any spectral density. We propose the simplest form of the leading pion BSA with its correct power law description. It is merely equivalent to taking the delta function to represent the spectral density in earlier models.

The QCD evolution of the pion DA is specified through the ERBL equations, derived in the Refs. [20,23,80]. It determines the logarithmic dependence of the DAs on ζ. At the leading order, the QCD evolution equations for the DAs can be expressed in terms of Gegenbauer polynomials [81]

TABLE I. Parameter values at 2 GeV, and the corresponding computed pion decay constant and the second moment.

y (GeV)	M (GeV)	f_π (GeV)	$\langle(2x-1)^2\rangle$
7	0.3105	0.0924	0.24
17	0.2580	0.0924	0.26

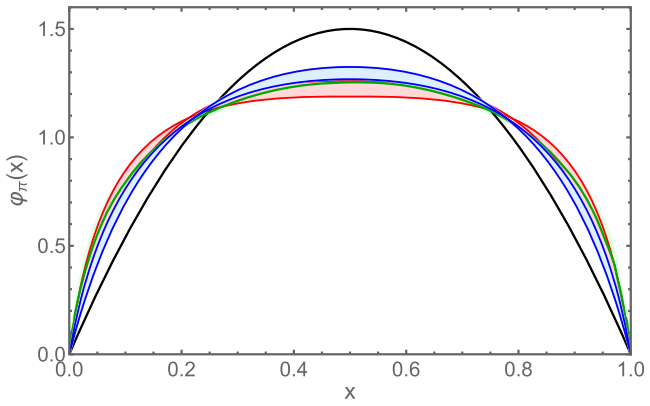

FIG. 2. DAs for π. The red band corresponds to our DA in Eq. (12) at 2 GeV. The blue-filled band represents evolved DA at the scale of $\zeta^2 = 60$ GeV^2. The solid black curve corresponds to the asymptotic DA $\phi_{asy}(x) = 6x(1-x)$. The green curve represents the SDE prediction of the DA at 2 GeV.

$$\varphi(x,\zeta) = 6x(1-x)\left(1+\sum_{n=1}^{\infty}a_n^\zeta C_n^{3/2}(2x-1)\right), \quad (10)$$

with $a_n^\zeta = a_n^{\zeta_2}(\alpha_s(\zeta)/\alpha_s(\zeta_2))^{-\gamma_n}$. Note that only even n contributes, and the anomalous dimensions are

$$\gamma_n = \frac{C_F}{\beta}\left(1+4\sum_{2}^{n+1}\frac{1}{k}-\frac{2}{(n+1)(n+2)}\right), \quad (11)$$

where we have $C_F = \frac{Nc^2-1}{2Nc}$, $\beta = \frac{11}{3}N_c - 2/3N_f$. Moreover, $\alpha_s(\zeta) = \frac{2\pi}{\beta\ln[\zeta/\Lambda_{\rm QCD}]}$, with $\Lambda_{\rm QCD} = 0.234$ GeV being the QCD scale parameter. Once the relevant coefficients a_n are determined, the evolution equation can be solved. These coefficients can be calculated using the initial conditions that the model calculation provides. By using initial DA $\varphi(x,\zeta_2 = 2\ \text{GeV})$ along with the Gegenbauer polynomials' orthogonality relation,

$$a_n^{\zeta_2} = \frac{2}{3}\frac{2n+3}{(n+1)(n+2)}\int_0^1 dx C_n^{3/2}(2x-1)\varphi(x,\zeta_2), \quad (12)$$

one is able to find the a_n coefficients. All model calculations should be consistent with the theoretical asymptotic behavior of the DA after evolution.

Clearly, our model at the scale of 2 GeV only depends on the parameters y and M. We now introduce the scale dependence of these parameters. The procedure is as follows: we employ leading-order QCD evolution Eq. (10) to obtain the evolved DA at a specific scale. Then, we refit the parameters y and M, keeping f_π unchanged, to generate a new DA that is equivalent to the evolved DA. We repeat this procedure at different scales and, ultimately, obtain the scale-dependent extrapolation of these parameters. The expressions for these models are as follows:

$$y(\zeta) = \frac{7 + 0.722(-4+\zeta^2) + 0.003(-4+\zeta^2)^2}{1 + 0.151(-4+\zeta^2) + 0.0007(-4+\zeta^2)^2},$$
$$M(\zeta) = \frac{0.3105 + 0.192(-4+\zeta^2) + 0.004(-4+\zeta^2)^2}{1 + 0.596(-4+\zeta^2) + 0.010(-4+\zeta^2)^2} \tag{13}$$

and

$$y(\zeta) = \frac{17 + 1.644(-4+\zeta^2) + 0.006(-4+\zeta^2)^2}{1 + 0.181(-4+\zeta^2) + 0.001(-4+\zeta^2)^2},$$
$$M(\zeta) = \frac{0.285 + 0.273(-4+\zeta^2) + 0.006(-4+\zeta^2)^2}{1 + 1.009(-4+\zeta^2) + 0.018(-4+\zeta^2)^2} \tag{14}$$

for the respective parameter sets. After the evolution, the DA takes a similar functional form as Eq. (12), but with explicit scale dependence, $\varphi(x,\zeta)$. Figure 2 depicts the slow evolution of the DA toward the asymptotic limit through a light-blue band.

IV. TRANSITION FORM FACTOR: $\gamma^*\pi^0\gamma$

A single scalar function is required to fully describe the amplitude for the transition $\gamma^*\pi^0\gamma$,

$$T_{\mu\nu}(k_1,k_2) = \frac{e^2}{4\pi^2 f_\pi}\epsilon_{\mu\nu\alpha\beta}k_{1\alpha}k_{2\alpha}G(k_1^2, k_1\cdot k_2, k_2^2), \tag{15}$$

where k_1 and k_2 are the photon momenta. The general impulse approximation for the transition amplitude of $\gamma^*\gamma \to \pi^0$ can be expressed as [82–84]

$$T_{\mu\nu}(k_1,k_2) = \frac{N_c}{3} tr \int_q i\Gamma_\nu(k_2)S(q-k_2) \times \Gamma_\pi(P)S(q+k_1)i\Gamma_\mu(k_1)S(q), \tag{16}$$

where $P = -(k_1+k_2)$ is the total momentum of the pion, such that $P^2 = -m_\pi^2$. The kinematic constraints are

$$k_1^2 = Q^2, \quad k_2^2 = Q'^2, \quad k_1\cdot k_2 = -(Q^2+Q'^2+m_\pi^2)/2. \tag{17}$$

By incorporating these kinematic constraints, the pion TFF is defined as (we only consider the singly virtual case, where $Q'^2 = 0$)

$$G^{\gamma^*\pi^0\gamma}(Q^2) = 2G(Q^2,0,0), \tag{18}$$

where the factor 2 appears in order to account for the two possible orderings of the photons. The other elements in Eq. (16) are the quark propagator, pion BSA, and the dressed QPV proposed in the previous sections. It is in principle straightforward to compute this transition. The isospin symmetry approximation, which assumes that up (u) and down (d) quarks have identical masses, is used.

We first consider the chiral limit and $Q^2 = 0$, which corresponds to calculating the chiral anomaly, i.e., $G(0,0,0)$, using Eq. (16). The first thing to notice is that the use of the bare vertex alone, i.e., $\eta = 0$, fails to reproduce the chiral anomaly. Introducing a more elaborate QPV, it is gathered that the AMM term contributes to the chiral anomaly. To quantify this statement, let us consider the $\eta = 0$ limit and calculate Eq. (16). In this limit, $G^{\eta=0}(0,0,0) \neq \frac{1}{2}$. Thus, the value specified by the chiral anomaly is not reproduced. Therefore, we fix the value of the strength parameter η to acquire $G(0,0,0) = \frac{1}{2}$. Within our choice of models for the quark propagator, QPV, the BSA, and the pion DA, we find that the chiral anomaly is faithfully reproduced, $G^{\eta=0.598(0.615)}(0,0,0) = \frac{1}{2}$, at 2 GeV with both parameter sets in Table I for slightly different values of $\eta = 0.598(0.615)$.

The results obtained through our calculations of the $\gamma^*\pi^0\gamma$ TFF in both cases are depicted in Fig. 3. It is clear that $G^{\gamma^*\pi^0\gamma}(Q^2)$ is a decreasing function of Q^2. It decreases rapidly for small values of Q^2, while it does so slowly for large values of Q^2. It is also evident that our results agree with the experimental data for the complete range of Q^2, wherever the results are available, and with the results reported in Refs. [82,85]. Pion's interaction radius is defined as

$$r_{\pi^0}^2 = -6\frac{d}{dQ^2}\ln g_{\pi\gamma\gamma}(Q^2)|_{Q^2=0}, \tag{19}$$

where $g_{\pi\gamma\gamma}(Q^2) = G(Q^2,0,0)$. Our computed interaction radii are bounded within the range

$$r_{\pi^0} \in (0.63, 0.67), \tag{20}$$

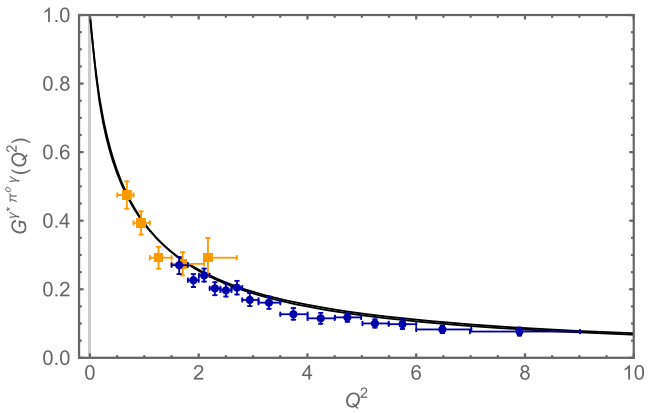

FIG. 3. The $\gamma^*\pi^0\gamma$ TFF. Pion TFF results are represented with the black band computed with Eq. (15) using the parameters in Table I. Data: CELLO [28]—squares (orange), and CLEO [29]—disks (blue).

where 0.63 corresponds to the first set of parameters and 0.67 to the second set of parameters. Moreover, we use $\hat{M} = 0.42$ GeV in the damping function. The experimental value, $r_{\pi^0} = 0.65 \pm 0.03$ fm [28], lies within this range, which is a positive result. On the other hand, in the limit $\eta = 0$,

$$r_{\pi^0} \in (0.53, 0.60), \tag{21}$$

which is considerably less than the experimental estimate. This observation implies that the presence of the AMM term in the QPV is crucial. For the sake of completeness, we also calculate the corresponding decay width,

$$\Gamma_{\pi^0\gamma\gamma} = \left.\frac{g^2_{\pi\gamma\gamma}(Q^2)\alpha^2_{em}m^3_\pi}{16\pi^3 f^2_\pi}\right|_{Q^2=0}, \tag{22}$$

where $\alpha_{\rm em} = 1/137$ is the fine-structure constant. The decay width produced by Eq. (22) is $\Gamma = 7.72$ eV with both parameter sets, which is in good agreement with the experimental value $\Gamma = 7.82 \pm 0.14 \pm 0.17$ eV [86]. We observe that the decay width is substantially sensitive to the pion mass. Therefore, we use the experimental value of this mass, i.e., $m_\pi = 134.9768 \pm 0.0005$ MeV [86].

Our calculated $Q^2 \times$ TFF is shown in Fig. 4. We present two results, one where we use parameters at 2 GeV (left panel), and the other with scale-dependent parameters (right panel). Our prediction is indicated by the light-blue band with parameters at 2 GeV and the light-red band with scale-dependent parameters. The asymptotic value of the pion TFF is $2f_\pi = 0.185$ GeV, plotted as the dotted (gray) curve. From the Figs. 3 and 4, we can observe that the functional behavior of our pion TFF is in agreement with perturbative QCD, which predicts constant behavior of the pion $Q^2 \times$ TFF at very large Q^2. However, our result slightly overshoots the asymptotic value. With the evolved parameters, we might expect numerical agreement with pQCD prediction, as we argue later in the text. Within the range of $Q^2 \leq 3$ GeV^2, pion TFF agrees with the available BESIII (preliminary) data, and it has the same behavior as experimental determination, within the error bars, in the 2 GeV$^2 \leq Q^2 \leq 8$ GeV^2 region. Figure 4 shows that the pion TFF has steeper Q^2 dependence in the range $Q^2 \leq$ 14 GeV^2 than the experimental measurements, and has good agreement with results from Belle collaboration beyond this range. The increase found by *BABAR* collaboration for $Q^2 \geq 10$ GeV^2 is not reproduced. In addition, there are theoretical studies speculating that the *BABAR* data might not be the exact representation of the pion TFF [33,87–89]. It is also shown in Ref. [32] that the *BABAR* data behavior at large Q^2 cannot be explained with QCD calculations by using the asymptotic QCD, AdS/QCD, and Chernyak-Zhitnitsky models for the DA, but can be supported by a flat modeling of the pion DA model [32,90], which significantly underestimates the pion TFF at low Q^2. These theoretical studies compute the pion TFF using different models of DA. Our approach has the added advantage that it produces the correct value of chiral anomaly while preserving satisfactory agreement with experimental data. Moreover, it incorporates quark confinement through the existence of complex conjugate mass poles. It also allows us to compute $G^{\gamma^*\pi^0\gamma}(Q^2)$ on the entire domain of Q^2 and produces the required $1/Q^2$ functional behavior of the TFF for $Q^2 \to \infty$, just as predicted by pQCD. Our DA model has good agreement with the earlier refined SDE predictions. The momentum evolution of our computed DA suggests an expected scaling violation, which we explain and quantify later in the text. On the other hand, there are also phenomenological studies that support the *BABAR* findings [91–95]. It is worth noting

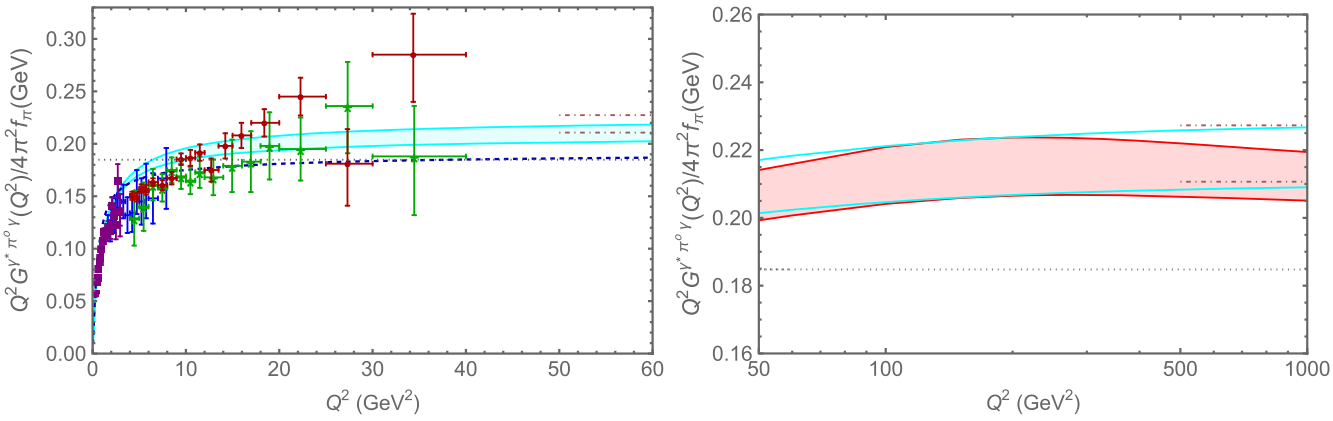

FIG. 4. Q^2-weighted $\gamma^*\pi^0\gamma$ TFF. Curves: blue dashed curve—result obtained from Eq. (15) using asymptotic DA $\phi_{asy}(x)$, gray dotted curve—the limit with asymptotic PDA input, and pink dot-dashed curve—related to the limit with the present model DA at 2 GeV input. Data: BESIII (preliminary) [96]—squares (purple), CLEO [29]—diamonds (blue), Belle [29]—stars (green), and *BABAR* [30]—disks (red). Left panel: $Q^2 G^{\gamma^*\pi^0\gamma}(Q^2)$ results are plotted with the light-blue band computed with Eq. (15) using parameters in Table I. Right panel: the light-red band corresponds to our $Q^2 G^{\gamma^*\pi^0\gamma}(Q^2)$ results using the evolved parameters.

that the π^0 TFF band calculated with evolved parameters touches the lower boundary of the TFF band calculated with parameters at 2 GeV. It also lies within the error bars of the experimental data.

Finally, let us decipher the large Q^2 limit of the pion TFF within the proposed QAM. The leading-order behavior is determined by using the bare QPV as input. By introducing Feynman parametrization and integrating over the momentum coordinate exactly, we can derive

$$G(Q^2) = 4M^4 y \sum_{j1,j2,j3} \int_T u_1^2 u_2 \frac{\mathcal{N}}{\mathcal{D}^2}, \tag{23}$$

with ($\int_T = \int_0^1 du_1 \int_0^1 du_2 \int_0^1 du_3$), and

$$\begin{aligned}\mathcal{N} = {} & (1+\beta)\alpha_{j1}\alpha_{j3}\beta_{j2} + (1-\alpha)\alpha_{j2}\alpha_{j3}\beta_{j1} \\ & + (1-\alpha+\beta)\alpha_{j2}\alpha_{j1}\beta_{j3},\end{aligned} \tag{24}$$

$$\begin{aligned}\mathcal{D} = {} & Q^2 2u_1(1-u_2)(1-\alpha) + 2y(1-u_1)M^2 \\ & + \gamma_{j1}M^2(1-2\alpha+u_1) \\ & + \gamma_{j2}M^2(-1+2\alpha-u_1+2u_1u_2) \\ & + \gamma_{j3}M^2 2u_1(1-u_2),\end{aligned} \tag{25}$$

where

$$\alpha = -\frac{1}{2}(-1+u_1(-1+2u_2u_3)), \tag{26}$$

$$\beta = -\frac{1}{2}(1+u_1+2u_1u_2(-1+u_3)). \tag{27}$$

Using the change of variable $u_3 = \frac{1-2\alpha+u1}{2u_1u_2}$, one can convert $\int_T$ to

$$\left\{\int_0^{\frac{1}{2}}\int_{1-2\alpha}^1 + \int_{\frac{1}{2}}^1\int_{-1+2\alpha}^1\right\} d\alpha du_1 \int_{\frac{1-2\alpha+u_1}{2u_1}}^1 \frac{du_2}{u_1u_2}. \tag{28}$$

Now, we integrate over u_2 and retain the leading-order term in powers of Q^2. Finally, integrating over u_1 by taking into account that $\sum \alpha_j = 1$ yields

$$G(Q^2) \to \frac{4\pi^2 f_\pi^2}{Q^2}\int_0^1 d\alpha \frac{\varphi(\alpha)}{3(1-\alpha)}, \tag{29}$$

where the DA $\varphi(\alpha)$ is defined through Eq. (12). We are thus able to explicitly derive the analytical expression of the TFF in the asymptotic limit within this model. It is

$$\exists\, Q_0 \gg m_p \left|\frac{1}{4\pi^2 f_\pi} Q^2 G^{\gamma^*\pi^0\gamma}(Q^2)\right. \overset{Q^2>Q_0^2}{\approx} 2f_\pi w(Q^2), \tag{30}$$

with $w(Q^2) = \int_0^1 \mathrm{d}x \frac{\varphi(x,Q^2)}{3(1-x)}$, and m_p is the proton mass. This behavior is fully consistent with the asymptotic QCD predication with the input DA, $\varphi(x, Q\to\infty) = 6x(1-x)$.

If we choose the specific scale of 2 GeV for the input quark propagator and the BSA for the computation of the DA, then we naturally expect a different Brodsky-Lepage (BL) limit, which is clearly marked in Fig. 4, dot-dashed curve, for both sets of parameters. Numerically, we obtain the BL limit to be $2.272 f_\pi$ and $2.466 f_\pi$ for parameter sets 1 and 2, respectively. Figure 4 shows that $Q^2 \times$ TFF increases with Q^2 and slightly overtakes the asymptotic limit of $2f_\pi$. At very large values of Q^2, $Q^2 \times$ TFF approaches our computed $Q^2 \to \infty$ limit from below.

With scale-dependent parameters, scaling violations are observed, as the evolution of the DA regulates the Q^2 dependence of the TFF. It naturally raises the question: at what value of Q_0 do scaling violations become apparent in this model? The right panel of Fig. 4 clearly shows that $Q_0 \sim 20$ GeV for our model, at which this scale violation starts to manifest itself. For Q exceeding Q_0, the $Q^2 \times$ TFF deceases very slowly, and we can expect it to approach $2f_\pi$ from above as $Q \to \infty$.

V. CONCLUSIONS

In this work, we computed the pion TFF $G^{\gamma^*\pi^0\gamma}(Q^2)$ for one real and one virtual photon. We employed models of the quark propagator, pion BSA, and the QPV instead of the solutions of the SDEs and BSEs of QCD. For completeness, we also calculated the pion interaction radius and the corresponding decay width. We modeled the expected momentum dependence of the quark propagator with a QAM, which captured the complex conjugate singularities on the complex momentum plane, which can be related to confinement. We constructed the BSA without a spectral density function, which encapsulated its low- and large-momentum behavior. We then obtained the pion DA by using the proposed quark propagator and the BSA. We then evolved it according to the ERBL evolution equation from perturbative QCD at the hadronic scale to complete the computation of the pion TFF. Our calculations were based on the bare as well as the dressed QPV, by adding the quark AMM term to the tree-level vertex. While both *Ansätze* of the QPV produced the same qualitative behavior of the pion TFF, the quark AMM term played an essential role to produce the correct chiral anomaly and the charge radius of the pion.

Note that the tree-level vertex failed to produce the chiral anomaly, which was associated with the on-shell photon and chiral limit pion, i.e., $G(0,0,0)$. The AMM term served as an effective term that contributed to normalizing the TFF. The strength parameter η could be tuned to produce the chiral anomaly, i.e., $G(0,0,0) = \frac{1}{2}$. The dressed QPV followed the asymptotic limit, i.e., $\Gamma_\mu(Q) \to \gamma_\mu$ as $Q^2 \to \infty$. It is clear from Fig. 3 that the AMM term

contributed significantly to the QPV in the low Q^2 domain. Its contribution virtually disappeared as Q^2 increased. As a result, the interaction radius and the decay width were consistent with the empirical findings.

We presented pion TFF results using the parameters at 2 GeV as well as using the evolved parameters. We found decent agreement with experimental data. However, we tended to disagree with the rapid increase in the large Q^2 region suggested by *BABAR* collaboration; instead, we had reasonable accordance with the Belle data. The computation at any desired value of spacelike Q^2 is an extra advantage of the QAM due to its simplicity. We also found that our numerical result for the pion TFF agreed well with BESIII (preliminary) data in the domain $Q^2 \leq 3$ GeV^2. It is hoped that the upcoming, more precise results from the planned Belle II experiment will help explain the previous discrepancies between experimental observations and theoretical predictions [38]. Our DA model had good agreement with the earlier SDE prediction, which lies within our proposed DA band. Due to the different scale, i.e., 2 GeV, our BL limit was larger than the asymptotic prediction limit, $2f_\pi$. However, our numerically computed pion TFF was clearly in agreement with our analytically calculated BL limit with both the parameter sets, and at very large Q^2, it approached the BL limit from below. The evolution of DA provided the phenomena of scaling violation, starting from $Q_0 \sim 20$ GeV, and TFF approached to $2f_\pi$ from above at $Q \to \infty$.

In conclusion, we suggested a model of the pion BSA that is simple but offers a powerful tool for the analysis of the electromagnetic properties, as well as a momentum-dependent model of the quark propagator that captures the confining features through related complex conjugate singularities. We also proposed a model for the PDA that has excellent agreement with the SDE predictions. The pion TFF results obtained with this compound QAM agreed well with the available experimental data and obeyed our computed BL limit at 2 GeV from below, which could be obtained analytically. Whereas with the evolution of DA, the pion TFF approached the asymptotic limit, $2f_\pi$, from above. Although the model is simple, without recourse to a spectral density function and with an added advantage of the momentum-dependent quark mass function with confinement mimicking complex conjugate singularities, it must be able to produce a large number of pion-related observables, such as the pion EFF, generalized parton distributions, and the parton distribution functions, at the experimental scale. It is also straightforward to extend the present work to the case of both photons being virtual with respected virtualities Q^2 and Q'^2. Considering this double virtuality case, we can define $\eta_+ = \frac{Q^2+Q'^2}{2}$ and $w = \frac{Q^2-Q'^2}{Q^2+Q'^2}$, with the latter quantifying the asymmetry in the virtuality of both photons. In this case, we can obtain a not too dissimilar large η_+ behavior of the transition form factor similar to the single virtuality case of Eq. (29),

$$\sim \frac{1}{\eta_+} \int_0^1 d\alpha \frac{\varphi(\alpha)}{1+(1-2\alpha)w}. \tag{31}$$

This is the generalized Brodsky-Lepage limit for the pseudoscalar meson transition form factor. Moreover, one can compute its effect on the anomalous magnetic moment of the muon through the hadron light-by-light scattering processes involving the neutron pion pole. All this is a case for future work.

ACKNOWLEDGMENTS

This work is financially supported by the National Natural Science Foundation of China (Grant No. 12135007). A. B. wishes to acknowledge the *Coordinación de la Investigación Científica* of the *Universidad Michoacana de San Nicolás de Hidalgo*, Morelia, Mexico, Grant No. 4.10, the *Consejo Nacional de Humanidades, Ciencias y Tecnologías*, Mexico, Project No. CBF2023-2024-3544, as well as the Beatriz-Galindo support during his current scientific stay at the University of Huelva, Huelva, Spain.

DATA AVAILABILITY

No data were created or analyzed in this study.

[1] H. Fritzsch, M. Gell-Mann, and H. Leutwyler, Advantages of the color octet gluon picture, Phys. Lett. **47B**, 365 (1973).
[2] D. J. Gross and F. Wilczek, Ultraviolet behavior of non-Abelian gauge theories, Phys. Rev. Lett. **30**, 1343 (1973).
[3] H. D. Politzer, Reliable perturbative results for strong interactions?, Phys. Rev. Lett. **30**, 1346 (1973).
[4] K. G. Wilson, Confinement of quarks, Phys. Rev. D **10**, 2445 (1974).
[5] F. J. Dyson, The radiation theories of Tomonaga, Schwinger, and Feynman, Phys. Rev. **75**, 486 (1949).
[6] J. S. Schwinger, On the Green's functions of quantized fields. I, Proc. Natl. Acad. Sci. U.S.A. **37**, 452 (1951).
[7] F. J. Dyson, The S matrix in quantum electrodynamics, Phys. Rev. **75**, 1736 (1949).
[8] C. D. Roberts and A. G. Williams, Dyson-Schwinger equations and their application to hadronic physics, Prog. Part. Nucl. Phys. **33**, 477 (1994).

[9] R. Alkofer and L. von Smekal, The infrared behavior of QCD Green's functions: Confinement dynamical symmetry breaking, and hadrons as relativistic bound states, Phys. Rep. **353**, 281 (2001).
[10] P. Maris and C. D. Roberts, Dyson-Schwinger equations: A tool for hadron physics, Int. J. Mod. Phys. E **12**, 297 (2003).
[11] C. S. Fischer, Infrared properties of QCD from Dyson-Schwinger equations, J. Phys. G **32**, R253 (2006).
[12] A. Bashir, L. Chang, I. C. Cloet, B. El-Bennich, Y.-X. Liu, C. D. Roberts, and P. C. Tandy, Collective perspective on advances in Dyson-Schwinger equation QCD, Commun. Theor. Phys. **58**, 79 (2012).
[13] K. Raya, A. Bashir, D. Binosi, C. D. Roberts, and J. Rodríguez-Quintero, Pseudoscalar mesons and emergent mass, Few Body Syst. **65**, 60 (2024).
[14] D. Binosi, L. Chang, J. Papavassiliou, S.-X. Qin, and C. D. Roberts, Symmetry preserving truncations of the gap and Bethe-Salpeter equations, Phys. Rev. D **93**, 096010 (2016).
[15] S. J. Brodsky and G. F. de Teramond, Light-front dynamics and AdS/QCD correspondence: The pion form factor in the space- and time-like regions, Phys. Rev. D **77**, 056007 (2008).
[16] L. Chang, I. Cloet, J. Cobos-Martinez, C. Roberts, S. Schmidt, and P. Tandy, Imaging dynamical chiral-symmetry breaking: Pion wave function on the light front, Phys. Rev. Lett. **110**, 132001 (2013).
[17] G. S. Bali, V. M. Braun, S. Bürger, M. Göckeler, M. Gruber, F. Hutzler, P. Korcyl, A. Schäfer, A. Sternbeck, and P. Wein (RQCD Collaboration), Light-cone distribution amplitudes of pseudoscalar mesons from lattice QCD, J. High Energy Phys. 08 (2019) 065; 11 (2020) 37.
[18] Z.-F. Cui, M. Ding, F. Gao, K. Raya, D. Binosi, L. Chang, C. D. Roberts, J. Rodríguez-Quintero, and S. M. Schmidt, Kaon and pion parton distributions, Eur. Phys. J. C **80**, 1064 (2020).
[19] N. G. Stefanis, Pion-photon transition form factor in light cone sum rules and tests of asymptotics, Phys. Rev. D **102**, 034022 (2020).
[20] G. P. Lepage and S. J. Brodsky, Exclusive processes in perturbative quantum chromodynamics, Phys. Rev. D **22**, 2157 (1980).
[21] V. L. Chernyak and A. R. Zhitnitsky, Asymptotic behavior of exclusive processes in QCD, Phys. Rep. **112**, 173 (1984).
[22] S. J. Brodsky and G. P. Lepage, Exclusive processes in quantum chromodynamics, Adv. Ser. Dir. High Energy Phys. **5**, 93 (1989).
[23] G. P. Lepage and S. J. Brodsky, Exclusive processes in quantum chromodynamics: Evolution equations for hadronic wavefunctions and the form factors of mesons, Phys. Lett. **87B**, 359 (1979).
[24] J. R. Forshaw and R. Sandapen, An AdS/QCD holographic wavefunction for the ρ meson and diffractive ρ meson electroproduction, Phys. Rev. Lett. **109**, 081601 (2012).
[25] F. Gao, L. Chang, Y.-X. Liu, C. D. Roberts, and S. M. Schmidt, Parton distribution amplitudes of light vector mesons, Phys. Rev. D **90**, 014011 (2014).
[26] B. El-Bennich, A. Furman, R. Kaminski, L. Lesniak, B. Loiseau, and B. Moussallam, *CP* violation and kaon-pion interactions in $B \to K\pi^+\pi^-$ decays, Phys. Rev. D **79**, 094005 (2009); **83**, 039903(E) (2011).
[27] C. Shi, C. Chen, L. Chang, C. D. Roberts, S. M. Schmidt, and H.-S. Zong, Kaon and pion parton distribution amplitudes to twist-three, Phys. Rev. D **92**, 014035 (2015).
[28] H. J. Behrend *et al.* (CELLO Collaboration), A measurement of the π^0, η and η' electromagnetic form-factors, Z. Phys. C **49**, 401 (1991).
[29] J. Gronberg, T. Hill, R. Kutschke, D. Lange, S. Menary, R. Morrison, H. Nelson, T. Nelson, C. Qiao, J. Richman *et al.*, Measurements of the meson-photon transition form factors of light pseudoscalar mesons at entum transfer, Phys. Rev. D **57**, 33 (1998).
[30] B. Aubert, Y. Karyotakis, J. Lees, V. Poireau, E. Prencipe, X. Prudent, V. Tisserand, J. G. Tico, E. Grauges, M. Martinelli *et al.*, Measurement of the $\gamma\gamma^* \to \pi^0$ transition form factor, Phys. Rev. D **80**, 052002 (2009).
[31] H. L. L. Roberts, C. D. Roberts, A. Bashir, L. X. Gutierrez-Guerrero, and P. C. Tandy, Abelian anomaly and neutral pion production, Phys. Rev. C **82**, 065202 (2010).
[32] S. J. Brodsky, F.-G. Cao, and G. F. de Teramond, Evolved QCD predictions for the meson-photon transition form factors, Phys. Rev. D **84**, 033001 (2011).
[33] A. P. Bakulev, S. V. Mikhailov, A. V. Pimikov, and N. G. Stefanis, Pion-photon transition: The new QCD frontier, Phys. Rev. D **84**, 034014 (2011).
[34] B. El-Bennich, J. P. B. C. de Melo, and T. Frederico, A combined study of the pion's static properties and form factors, Few Body Syst. **54**, 1851 (2013).
[35] S. Uehara *et al.* (Belle Collaboration), Measurement of $\gamma\gamma^* \to \pi^0$ transition form factor at Belle, Phys. Rev. D **86**, 092007 (2012).
[36] K. Raya, L. Chang, A. Bashir, J. J. Cobos-Martinez, L. X. Gutiérrez-Guerrero, C. D. Roberts, and P. C. Tandy, Structure of the neutral pion and its electromagnetic transition form factor, Phys. Rev. D **93**, 074017 (2016).
[37] I. M. Higuera-Angulo, R. J. Hernández-Pinto, K. Raya, and A. Bashir, Electromagnetic and two-photon transition form factors of the pseudoscalar mesons: An algebraic model computation, Phys. Rev. D **110**, 034013 (2024).
[38] W. Altmannshofer *et al.* (Belle-II Collaboration), The Belle II physics book, Prog. Theor. Exp. Phys. **2019**, 123C01 (2019); **2020**, 029201(E) (2020).
[39] G. Eichmann, C. S. Fischer, E. Weil, and R. Williams, Single pseudoscalar meson pole and pion box contributions to the anomalous magnetic moment of the muon, Phys. Lett. B **797**, 134855 (2019); **799**, 135029(E) (2019).
[40] K. Raya, A. Bashir, and P. Roig, Contribution of neutral pseudoscalar mesons to a_μ^{HLbL} within a Schwinger-Dyson equations approach to QCD, Phys. Rev. D **101**, 074021 (2020).
[41] T. Aoyama *et al.*, The anomalous magnetic moment of the muon in the standard model, Phys. Rep. **887**, 1 (2020).
[42] E. E. Salpeter and H. A. Bethe, A relativistic equation for bound-state problems, Phys. Rev. **84**, 1232 (1951).
[43] M. Gell-Mann and F. Low, Bound states in quantum field theory, Phys. Rev. **84**, 350 (1951).
[44] C. D. Roberts and A. G. Williams, Dyson-Schwinger equations and their application to hadronic physics, Prog. Part. Nucl. Phys. **33**, 477 (1994).
[45] R. Alkofer and L. Von Smekal, The infrared behaviour of QCD Green's functions: Confinement, dynamical symmetry

breaking, and hadrons as relativistic bound states, Phys. Rep. **353**, 281 (2001).
[46] A. Bashir, L. Chang, I. C. Cloet, B. El-Bennich, Y.-X. Liu, C. D. Roberts, and P. C. Tandy, Collective perspective on advances in Dyson–Schwinger equation QCD, Commun. Theor. Phys. **58**, 79 (2012).
[47] I. G. Aznauryan, A. Bashir, V. M. Braun, S. J. Brodsky, V. D. Burkert, L. Chang, C. Chen, B. El-Bennich, I. C. Cloet, P. L. Cole *et al.*, Studies of nucleon resonance structure in exclusive meson electroproduction, Int. J. Mod. Phys. E **22**, 1330015 (2013).
[48] P. Maris and C. D. Roberts, Dyson–Schwinger equations: A tool for hadron physics, Int. J. Mod. Phys. E **12**, 297 (2003).
[49] A. Höll, C. Roberts, and S. Wright, Hadron physics and Dyson-Schwinger equations, arXiv:nucl-th/0601071.
[50] C. D. Roberts, M. Bhagwat, A. Höll, and S. Wright, Aspects of hadron physics, Eur. Phys. J. Special Topics **140**, 53 (2007).
[51] M. A. Sultan, K. Raya, F. Akram, A. Bashir, and B. Masud, Effect of the quark-gluon vertex on dynamical chiral symmetry breaking, Phys. Rev. D **103**, 054036 (2021).
[52] R. Alkofer, W. Detmold, C. Fischer, and P. Maris, Analytic properties of the Landau gauge gluon and quark propagators, Phys. Rev. D **70**, 014014 (2004).
[53] R. Alkofer, W. Detmold, C. Fischer, and P. Maris, Analytic structure of the gluon and quark propagators in Landau gauge QCD, Nucl. Phys. B, Proc. Suppl. **141**, 122 (2005).
[54] R. Alkofer, C. S. Fischer, F. J. Llanes-Estrada, and K. Schwenzer, The quark–gluon vertex in landau gauge QCD: Its role in dynamical chiral symmetry breaking and quark confinement, Ann. Phys. (Amsterdam) **324**, 106 (2009).
[55] C. S. Fischer, Non-perturbative propagators, running coupling and dynamical mass generation in ghost-antighost symmetric gauges in QCD, arXiv:hep-ph/0304233.
[56] A. Cucchieri and T. Mendes, What's up with IR gluon and ghost propagators in Landau gauge? A puzzling answer form huge lattices, Proc. Sci. LATTICE2007 (**2007**) 297.
[57] J. Skullerud, P. O. Bowman, A. Kizilersü, D. B. Leinweber, and A. G. Williams, Nonperturbative structure of the quark-gluon vertex, J. High Energy Phys. 04 (2003) 047.
[58] J. Skullerud and A. Kizilersü, Quark-gluon vertex from lattice QCD, J. High Energy Phys. 09 (2002) 013.
[59] J.-I. Skullerud, P. O. Bowman, A. Kizilersu, D. B. Leinweber, and A. G. Williams, Quark-gluon vertex in arbitrary kinematics, Nucl. Phys. B, Proc. Suppl. **141**, 244 (2005).
[60] L. Chang, C. Mezrag, H. Moutarde, C. D. Roberts, J. Rodríguez-Quintero, and P. C. Tandy, Basic features of the pion valence-quark distribution function, Phys. Lett. B **737**, 23 (2014).
[61] L. Albino, I. Higuera-Angulo, K. Raya, and A. Bashir, Pseudoscalar mesons: Light front wave functions, GPDs, and PDFs, Phys. Rev. D **106**, 034003 (2022).
[62] L. Chang, A perspective on Dyson-Schwinger equation: Toy model of pion, EPJ Web Conf. **113**, 05001 (2016).
[63] L. Chang, I. C. Cloët, C. D. Roberts, S. M. Schmidt, and P. C. Tandy, Pion electromagnetic form factor at spacelike momenta, Phys. Rev. Lett. **111**, 141802 (2013).
[64] J. S. Ball and T.-W. Chiu, Analytic properties of the vertex function in gauge theories. I, Phys. Rev. D **22**, 2542 (1980).
[65] M. Bando, M. Harada, and T. Kugo, External gauge invariance and anomaly in BS vertices and bound states, Prog. Theor. Phys. **91**, 927 (1994).
[66] P. Maris and C. D. Roberts, Pseudovector components of the $\pi^0 \to \gamma\gamma$, and $F_\pi(q^2)$. Phys. Rev. C **58**, 3659 (1998).
[67] L. Albino, A. Bashir, L. X. G. Guerrero, B. E. Bennich, and E. Rojas, Transverse Takahashi identities and their implications for gauge independent dynamical chiral symmetry breaking, Phys. Rev. D **100**, 054028 (2019).
[68] A. Bashir, R. Bermudez, L. Chang, and C. D. Roberts, Dynamical chiral symmetry breaking and the fermion–gauge-boson vertex, Phys. Rev. C **85**, 045205 (2012).
[69] P. Maris and P. C. Tandy, The quark photon vertex and the pion charge radius, Phys. Rev. C **61**, 045202 (2000).
[70] H. Dang, Z. Xing, M. A. Sultan, K. Raya, and L. Chang, Chiral anomaly and the pion transition form factor: Beyond the cutoff, Phys. Rev. D **108**, 054031 (2023).
[71] S.-X. Qin, L. Chang, Y.-X. Liu, C. D. Roberts, and S. M. Schmidt, Practical corollaries of transverse Ward-Green-Takahashi identities, Phys. Lett. B **722**, 384 (2013).
[72] L. Chang, Y.-X. Liu, and C. D. Roberts, Dressed-quark anomalous magnetic moments, Phys. Rev. Lett. **106**, 072001 (2011).
[73] S. J. Brodsky and G. F. de Teramond, Light-front dynamics and AdS/QCD correspondence: The pion form factor in the space-and time-like regions, Phys. Rev. D **77**, 056007 (2008).
[74] S. Mikhailov, A. Pimikov, and N. Stefanis, Systematic estimation of theoretical uncertainties in the calculation of the pion-photon transition form factor using light-cone sum rules, Phys. Rev. D **93**, 114018 (2016).
[75] N. Stefanis, Pion-photon transition form factor in light cone sum rules and tests of asymptotics, Phys. Rev. D **102**, 034022 (2020).
[76] X. Gao, A. D. Hanlon, N. Karthik, S. Mukherjee, P. Petreczky, P. Scior, S. Syritsyn, and Y. Zhao, Pion distribution amplitude at the physical point using the leading-twist expansion of the quasi-distribution-amplitude matrix element, Phys. Rev. D **106**, 074505 (2022).
[77] L. Chang, I. C. Cloet, J. J. Cobos-Martinez, C. D. Roberts, S. M. Schmidt, and P. C. Tandy, Imaging dynamical chiral symmetry breaking: Pion wave function on the light front, Phys. Rev. Lett. **110**, 132001 (2013).
[78] S.-S. Xu, L. Chang, C. D. Roberts, and H.-S. Zong, Pion and kaon valence-quark parton quasidistributions, Phys. Rev. D **97**, 094014 (2018).
[79] C. D. Roberts, D. G. Richards, T. Horn, and L. Chang, Insights into the emergence of mass from studies of pion and kaon structure, Prog. Part. Nucl. Phys. **120**, 103883 (2021).
[80] S. J. Brodsky and G. P. Lepage, Exclusive processes and the exclusive-inclusive connection in quantum chromodynamics, Technical Report, SLAC National Accelerator Lab, Cornell University, Menlo Park, CA (United States), 1979.
[81] A. Courtoy, Generalized parton distributions of pions. spin structure of hadrons, arXiv:1010.2974.
[82] P. Maris and P. C. Tandy, Electromagnetic transition form factors of light mesons, Phys. Rev. C **65**, 045211 (2002).

[83] K. Raya, L. Chang, A. Bashir, J. J. Cobos-Martinez, L. X. Gutiérrez-Guerrero, C. D. Roberts, and P. C. Tandy, Structure of the neutral pion and its electromagnetic transition form factor, Phys. Rev. D **93**, 074017 (2016).
[84] H. Dang, Z. Xing, M. A. Sultan, K. Raya, and L. Chang, The chiral anomaly and the pion transition form factor: Beyond the cutoff, Phys. Rev. D **108**, 054031 (2023).
[85] J. Chen, M. Ding, L. Chang, and Y.-x. Liu, Two-photon transition form factor of $c^{-}c$ quarkonia, Phys. Rev. D **95**, 016010 (2017).
[86] R. L. Workman *et al.* (Particle Data Group Collaboration), Review of particle physics, Prog. Theor. Exp. Phys. **2022**, 083C01 (2022).
[87] H. Roberts, C. Roberts, A. Bashir, L. Gutiérrez-Guerrero, and P. Tandy, Abelian anomaly and neutral pion production, Phys. Rev. C **82**, 065202 (2010).
[88] S. V. Mikhailov and N. G. Stefanis, Pion transition form factor at the two-loop level vis-a-vis experimental data, Mod. Phys. Lett. A **24**, 2858 (2009).
[89] X.-G. Wu and T. Huang, Constraints on the light pseudoscalar meson distribution amplitudes from their meson-photon transition form factors, Phys. Rev. D **84**, 074011 (2011).
[90] M. V. Polyakov, On the pion distribution amplitude shape, JETP Lett. **90**, 228 (2009).
[91] X.-G. Wu and T. Huang, An implication on the pion distribution amplitude from the pion-photon transition form factor with the new *BABAR* data, Phys. Rev. D **82**, 034024 (2010).
[92] P. Kroll, The form factors for the photon to pseudoscalar meson transitions—an update, Eur. Phys. J. C **71**, 1623 (2011).
[93] E. Ruiz Arriola and W. Broniowski, Pion transition form factor in the Regge approach and incomplete vector-meson dominance, Phys. Rev. D **81**, 094021 (2010).
[94] S. S. Agaev, V. M. Braun, N. Offen, and F. A. Porkert, Light cone sum rules for the $\pi^0\gamma^*\gamma$ form factor revisited, Phys. Rev. D **83**, 054020 (2011).
[95] M. Gorchtein, P. Guo, and A. P. Szczepaniak, Form factors of pseudoscalar mesons, Phys. Rev. C **86**, 015205 (2012).
[96] C. F. Redmer, Measurements of hadronic and transition form factors at BESIII, EPJ Web Conf. **212**, 04004 (2019).